Available online at www.sciencedirect.com
SCIENCE DIRECT®
Journal of Nuclear Materials 337–339 (2005) 1064–1068
journal of nuclear materials
www.elsevier.com/locate/jnucmat

Surface temperature measurements of carbon materials in fusion devices

D. Hildebrandt *, D. Naujoks, D. Sünder

EURATOM Association Max-Planck-Institut für Plasmaphysik, Teilinstitut Greifswald, Wendelsteinstaße 1, 17491 Greifswald, Germany

Abstract

The accuracy of temperature measurements of carbon materials at surface heat loading using IR cameras operating in different wave length regions has been examined. Temperature excursions measured with high spatial and temporal resolution on virgin and plasma exposed samples during and after heat pulses by laser radiation are compared with values of the analytical and numerical solution of the heat diffusion equation. Deviations between measured and calculated results are found already on unexposed samples which can be mostly due to morphological effects. They are more pronounced for shorter wavelength regions. In addition the change of the temperature excursion after surface modification by plasma exposure has been investigated.

PACS: 44.50; 44.30; 44.10
Keywords: Carbon based materials; Divertor tiles; Laser application; Power deposition; IR thermography

1. Introduction

IR measurements using radiation between 0.5 and 5 μm have been applied on magnetic fusion devices in order to supervise and diagnose the power loading of plasma facing components with a spatial resolution of some millimetre [1]. During plasma exposure, however, the surface of the targets is modified by erosion and deposition processes influencing the surface temperature measurements and the accuracy of values of derived power flux densities [2–7].

In order to check both, the accuracy of temperature measurements and uncertainties of the values of derived power fluxes experiments involving well defined heat pulses by laser radiation [8–10] on carbon target materials including fine grained graphite (FGG) and carbon fiber composites (CFC) of different surface roughness and surface impurity contamination obtained after plasma exposure have been performed.

The surface temperature excursion during and after the laser heat pulse has been measured by three different cameras operating in the near (NIR), middle (MIR) and far infrared (FIR) wavelength region. To validate the accuracy of the measured surface temperature evolutions they are compared with corresponding values of analytic and numerical solutions of the three-dimensional heat diffusion equation.

2. Experimental

Carbon samples were prepared from the CFC material (SEBCARB N11) and from the FGG material

* Corresponding author.
E-mail address: dieter.hildebrandt@ipp.mpg.de (D. Hildebrandt).

0022-3115/$ - see front matter © 2004 Elsevier B.V. All rights reserved.
doi:10.1016/j.jnucmat.2004.09.033

(EK98). The surface morphology of all samples was characterized by the mean surface roughness measured by a laser profilometer (UBM). The CFC samples have a mean surface roughness of 15 μm. Most samples of fine grain graphite were examined with its original surface roughness ρ of about 5 μm while one sample was polished ($\rho = 0.4$ μm). In addition a FGG sample (Schunk- fp 479) cut from a tile of the ASDEX-Upgrade divertor IIb was investigated. This sample was located in the deposition dominated private flux region of the outer divertor near the separatrix position for 2 years of operation. It has a mean surface roughness of 2.1 μm after the plasma exposure. Surface analysis of this sample yielded a contamination layer with a thickness varying between 3 and 5 μm across the surface and consisting mainly of carbon, boron, deuterium and hydrogen.

All samples were irradiated by light of wavelength 1.06 μm from a pulsed Nd:YAG laser or by light of wavelength 807 nm from a cw diode laser.

The light pulses of the Nd:YAG laser have a spatial Gaussian profile with a standard deviation σ of 1–2 mm and a duration τ of up to 20 ms [9]. Heat fluxes with central densities P_0 up to 100 M/m^2 can be applied. The actual central heat flux density has been calibrated by combining three different measurements. The total absorbed energy (P_0*2π*σ*τ) was measured using small specimens of the investigated materials as a calorimeter for single pulses. The spatial distribution of the heat flux (σ) has been examined by the surface temperature distribution response of uniform materials as silicon and polished graphite at the beginning of the pulse and the temporal evolution (τ) was checked by time traces of randomly scattered laser light signals detected by a fast laser power meter.

The surface temperature excursion during and after the heat pulses was measured by IR cameras operating in the wavelength region between 3 and 5 μm (InSb detector array with 256 × 320 pixels) or 8–15 μm (VO_x-microbolometer array with 240 × 320 pixels). In addition, images have been taken in the wavelength region of 0.4–0.9 μm by a CCD camera (Si-array with 768 × 576 pixels). All cameras were calibrated versus black body radiation. Using microscopic lenses the spatial resolution has been improved to up to 30 μm/pixel (3–5 μm), 44 μm/pixel (8–15 μm) or 45 μm/pixel (0.4–0.9 μm). The thermal images have been taken with frame rates of 50 Hz (CCD and VO_x camera) and up to 6 kHz (InSb camera) at reduced image size.

3. Modelling

The starting point is the time dependent 3D heat conduction equation for the temperature in Cartesian coordinates $T(x, y, z, t)$ without a source term. For simplicity the heat conduction coefficient λ, the heat diffusion coefficient κ and the specific heat capacity c_p are assumed to be constant. The laser pulse at the surface of a semi-infinite target gives the boundary condition $-\kappa dT/dx = P$ at $x = 0$. The other boundaries of the target are thermally insulated.

Using the Fourier-Integral technique [11] the heat conduction equation has been solved with a Gaussian shaped heat pulse. For the central region of the laser spot ($x = y = z = 0$) and the condition $\lambda_{y,z} = \lambda_y = \lambda_z$ the solution is given by Eq. (1).

$$T - T_0 = \frac{\sqrt{2}}{\sqrt{\pi}} * \frac{\sigma * P_0}{\sqrt{\lambda_x * \lambda_{y,z}}} * \left[\arctan\left(\sqrt{\frac{2\kappa_{y,z} * t}{\sigma^2}} \right) - \Theta(t-\tau) * \arctan\left(\sqrt{\frac{2\kappa_{y,z} * (t-\tau)}{\sigma^2}} \right) \right]. \quad (1)$$

Here is $\Theta(t-\tau)$ the Heaviside function. The first term on the right describes the temperature increase during the laser pulse, while both terms together describe the successive temperature decay after the pulse.

Numerical calculations have been done using the codes THERM [8] and THEODOR [3]. Values of the heat conduction coefficient for the different carbon materials have been determined in separate experiments [8]. The THEODOR code uses a boundary condition which can simulate a surface layer with a heat conductivity which is different from λ of the bulk material.

4. Results

Fig. 1 shows in the upper part thermal images of the polished and unpolished FGG and the CFC material taken by the InSb camera during application of similar heat pulses at oblique incidence. The lateral surface temperature distribution of the polished fine grain graphite is very smooth and shaped slightly by the profile of the incident heat pulse, whereas that of the other materials is non-uniform with a texture size comparable to the spatial resolution of 30 μm. In the lower part of this figure the temperature distribution along the marked lines at the end of the heat pulse is seen. The temporal evolution of the temperature found for the CFC and the unpolished FGG material in diverse surface areas is quite different as shown in Fig. 2 for the CFC material. The combined values of a large area simulate measurements with a spatial resolution of 1×0.5 mm^2. The data are taken from the centre of the laser spot and are compared with the analytical solution (Eq. (1)) using the room temperature values of $c_p = 770$ J/kg K, $\lambda_x = 130$ W/km and $\lambda_{y,z} = 230$ W/km [8] and with the relation $\kappa = \lambda/\rho * c_p$. The temperature increase for the averaged values differs from the calculated one by a factor of about two at the end of the pulse. The deviation is even higher at former time.

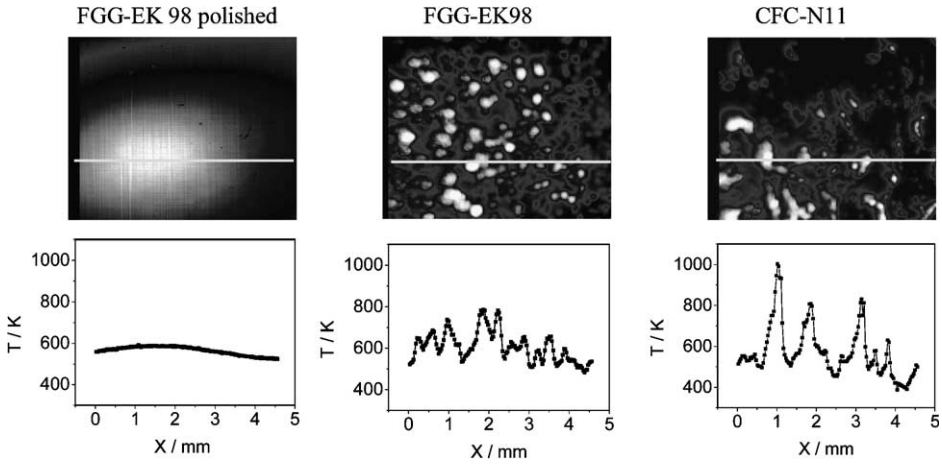

Fig. 1. Top: Thermal images taken by the InSb camera during laser pulses at oblique incidence with a spatial resolution of 30 μm/pixel and a temporal resolution of 1 ms; applied heat pulse $P_0 = 28$ (FGG) or 36 MW/m^2 (CFC), $\tau = 4$ ms, $\sigma = \mathrm{sqrt}(\sigma_y * \sigma_z) = 2$ mm; bottom: temperature distribution along the marked lines.

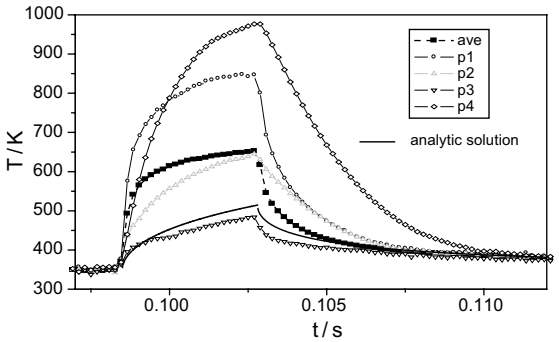

Fig. 2. Temperature excursions measured at different positions for the CFC material (Fig. 1) with a time resolution of 190 μs. The dashed curve is obtained by combining the signals from an area of 1×0.5 mm^2 simulating a lower spatial resolution. The solid curve is the analytic solution.

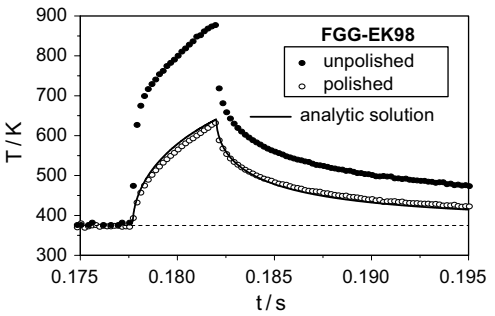

Fig. 3. Comparison of the surface temperature excursion measured by the InSb camera at the centre of the laser spot with results of the analytic solution for the polished and unpolished fine grain graphite. EK98; applied heat pulse $P_0 = 44$ MW/ m^2, $\tau = 4$ ms, $\sigma = 1.5$ mm.

Fig. 3 shows the temporal evolution of the surface temperature for the unpolished and polished FGG material EK98 as measured by the InSb camera with a spatial resolution of 0.4 mm during and after a heat pulse of duration 4 ms. The data are taken from the centre of the laser spot and are also compared with the analytical solution [Eq. (1)]. In this case $c_p = 770$ J/kg K and $\lambda = 110$ W/km are used. The temperature excursion measured for the polished material agrees with the corresponding values from the analytic solution very well. In contrast, for the unpolished sample, significant deviations have been found and in this particular case also for a long period after the heat pulse. Other unpolished FGG samples showed a somewhat better agreement after the heat pulse.

Fig. 4 shows the central heat flux density calculated by the THERM code for the polished and unpolished fine grain graphite. The input for the code calculations are the measured temporal evolutions of the surface temperature shown in Fig. 3. The calculated values of the heat flux density agree within 10% with the actual one for the polished material. But they are a factor of three higher at the beginning of the pulse and a factor of two at the termination for the unpolished material. This deviation corresponds to the fact that the measured temperature excursion is found to be much stronger than the analytically predicted one (see Fig. 3).

A similar qualitative temporal behaviour of a strongly decreasing heat flux was also calculated for the CFC material by both codes THERM and THEODOR. Taking into consideration a surface region with

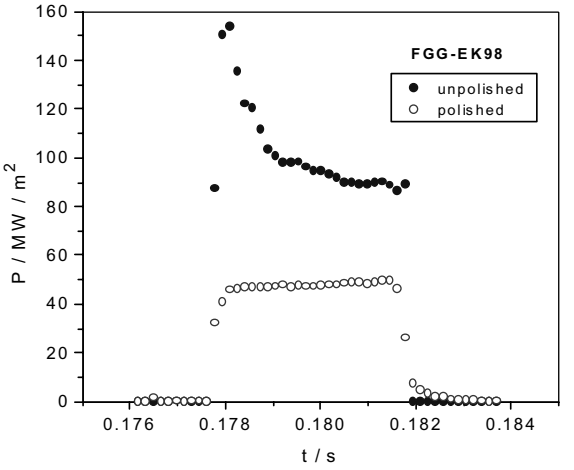

Fig. 4. Temporal evolution of the central heat flux density for a polished and an unpolished graphite sample calculated by the THERM code using the temperature values of Fig. 3; applied heat pulse $P_0 = 44$ MW/m^2, $\tau = 4$ ms, $\sigma = 1.5$ mm.

smaller heat conductivity than that of the bulk material the qualitative behaviour of the temporal evolution of the heat flux density could be well reproduced by the THEODOR code but the absolute value is then calculated to be a factor of two smaller than the actual heat flux density [9].

The influence of contamination layers on the measured temperature increase at surface heat loading was investigated for the FGG divertor piece of ASDEX-Upgrade. The sample was irradiated by light from the diode laser. The Gaussian shaped profile of the heat flux has a standard deviation of 0.36 mm. Fig. 5 shows the temperature excursion at three different spots. The distance between the spots is about 3 mm and the thickness of the contamination varies from spot to spot between 3 μm (spot 1) and 5 μm (spot 3). With such deposited surface layers the temperature pattern is rather uniform. Nevertheless, these measurements were performed by the VO_x-microbolometer camera to reduce any non-uniform effects (see below).

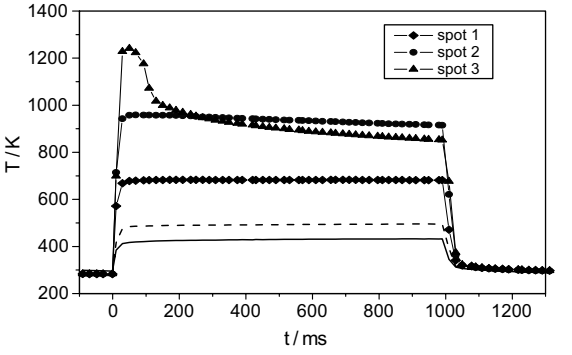

Fig. 5. Surface temperature excursion at three different spots on a contaminated sample and at a spot on the uncontaminated backside (dashed line) of the divertor target of ASDEX Upgrade measured by the VO_x camera with a spatial resolution of 90 μm; The thickness of the contamination is 3 μm (spot1), 4 μm (spot2) and 5 μm (spot3); applied heat pulse $P_0 = 28$ MW/m^2, $\tau = 1$ s, $\sigma = 0{,}36$ mm. The values of the solid line are calculated foraheat conductivity of this material $\lambda = 100$ W/km.

For comparison the temperature excursion observed on the virgin backside of this sample and the calculated results are also shown. On the unexposed sample backside the temperature increase have been measured to be 180 K about 30% higher than calculated. For the different spots on the plasma exposed surface the temperature increase was found to be between 400 K and 1000 K depending on the local surface conditions.

5. Discussion

The strongly textured surface temperature pattern during the heat pulse (Fig. 1) gives strong evidence of extremely spatial variation of thermal properties at the surface. This variation influences the accuracy of temperature measurements with insufficient spatial resolution. The measured temperature value results from a combination of various radiation components appearing from different areas [9,10] and depends on the wavelength at which the measurements are made [9,12].

The emitted power density shows a linear dependence on the temperature in the region of 8–15 μm and depends strongly on the temperature in the shorter wavelength regions [9]. This implies that signals from hot surface elements contribute predominantly to superimposed signals. With the CCD camera only the hottest spots are visible. The effect results in an overestimation of the averaged temperature value. It is demonstrated in Table 1 for the temperature distributions shown in Fig. 1 considered as a characteristic material feature. The values are estimated by integration of Wien's approximation of the Planck formulae and taking the sensitivity band of the cameras. The combined signal measured by the VO_x-microbolometer camera with poor

Table 1
Temperature values that would be obtained by line integrated measurements (spatial resolution of 4 mm) with cameras operating at different wavelengths for the temperature distribution of Fig. 1[a]

T/K	FGG-EK98-pol.	FGG-EK98	CFC-N11
VO_x (8–15 μm)	564	608	575
InSb (3–5 μm)	565	624	625
CCD (0.5–0.9 μm)	571	689	800

[a] The spectral sensitivity of the photovoltaic InSb and CCD (Si) sensors is ignored.

spatial resolution well approaches the mean value for the temperature distribution [9]. The most pronounced deviation is observed for the CCD camera and the CFC material with the highest surface roughness.

Both effects, the elevated mean surface temperature caused by the variation of the thermal conductivity across the surface and the overestimation of this value by the InSb camera explain the discrepancies between measured and calculated values by about 100% for the CFC material observed at insufficient spatial resolution as demonstrated in Fig. 2. Measurements in the far infrared region yielded lower discrepancies (see also [9]). The same explanation can be applied to the results for the unpolished FGG material (Figs. 3 and 4). However, the slow temperature decrease after the heat pulse found for the unpolished FGG sample in Fig. 3 cannot be satisfactorily described. Measurements on other FGG samples in the far infrared region indicate mostly a 30% lower mean value of the thermal conductivity for unpolished surfaces compared to that for the bulk material (see also Fig. 5).

Fig. 5 demonstrates the strong influence of the thickness of the contamination on the temperature increase at surface heat loading. A continuous decrease of the measured surface temperature (spots 2 and 3) indicates outgassing and partial removal of this contamination during the heat pulse (see also [7]). The measured temperature decreased below 1000 K after periods depending on the layer thickness, at the latest after 150 ms for the 5 μm thick contamination. At this temperature level the deuterium desorption rate of contaminated graphite divertor tiles was found to be strongly increased [13]. Post mortem surface analysis of the central region of spot 3 has shown this removal of the contamination. However, the thermal behaviour of strongly eroded or damaged surface parts differs from that of the original material at heat loading indicating a much lower thermal conductivity in damaged surface regions [7]. Further remarkably, the temperature level of spot 2 is higher at the termination of the heat pulse than that of spot 3, whereas it was lower at the beginning. This observation points out the influence of the thermal history. Careful interpretation of thermographic data must include separate evaluation for each camera pixel in certain cases and needs knowledge of the actual local surface heat conductivity (see also [2,4–6]). Measurements of the temperature evolution after surface heat loading with an adequate time resolution can give some information. On the other hand, the complication arises when the surface heat conductivity changes during long term or stationary discharges.

6. Conclusions

IR measurements performed in the MIR and NIR with insufficient spatial resolution show inaccuracies in surface temperature readings.

Values of the temperature excursion measured at surface heat loading for CFC material in the MIR differ by a factor of 2 from calculated ones.

FIR measurements are more accurate. They indicate mostly a 30% lower mean value of the thermal conductivity at the surface than in the bulk material for unpolished FGG material.

In plasma experiments, both the surface morphology and the thickness of contamination layers are continuously modified in an ill-defined manner due to erosion and deposition processes. The involved variation of the surface heat conductivity causes strong variation of the surface temperature and makes it difficult to supervise the power load of such surfaces during plasma exposure by thermography in real time. However, the observed removal of plasma deposited surface contaminations at surface heat loading is encouraging and seems to allow temperature supervising of components with a response time larger than 1 sec and critical surface temperatures higher than 1300 K.

References

[1] T. Eich, these Proceedings. doi:10.1016/j.jnucmat.2004.09.051.
[2] S. Clement et al., J. Nucl. Mater. 266–269 (1999) 285.
[3] A. Herrmann, in: Proceedings of 28th EPS Conference on Controlled Fusion and Plasma Physics, June 2001, Madeira (Portugal).
[4] P. Andrew et al., J. Nucl. Mater. 313–316 (2003) 135.
[5] Y. Corre et al., in: Proceedings of 30th EPS Conference on Controlled Fusion and Plasma Physics, July 2003, St. Petersburg (Russia).
[6] E. Gauthier et al., these Proceedings. doi:10.1016/j.jnucmat.2004.10.161.
[7] D. Hildebrandt et al., in: Proceedings of 31st EPS Conference on Controlled Fusion and Plasma Physics, June 2004, London (Great Britain).
[8] D. Hildebrandt et al., J. Nucl. Mater. 313–316 (2003) 738.
[9] D. Hildebrandt et al., in: InfraMation 2003 Proceedings, vol. 4, Las Vegas (USA), October, 2003.
[10] A. Herrmann et al., in: 10th Carbon Workshop, Jülich (Germany), September, 2003.
[11] G. Korn, M. Korn, Mathematical Handbook for Scientists and Engineers, MGraw-Hill Book Company Inc., 1961.
[12] R. Reichle et al., J. Nucl. Mater. 313–316 (2003) 711.
[13] D. Hildebrandt et al., J. Nucl. Mater. 266–269 (1999) 532.